Structure effects on the Coulomb dissociation of ^{8}B at relativistic energies

R. Shyam¶, K. Bennaceur†, J. Okołowicz†‡ and M. Ploszajczak†

¶ *Saha Institute of Nuclear Physics, 1/AF Bidhan Nagar, Calcutta - 700 064, India*

† *Grand Accélérateur National d'Ions Lourds (GANIL), CEA/DSM – CNRS/IN2P3, BP 5027,*
F-14076 Caen Cedex 05, France

‡ *Institute of Nuclear Physics, Radzikowskiego 152, PL - 31342 Kraków, Poland*

Abstract

We investigate the Coulomb dissociation of ^{8}B on ^{208}Pb target at the beam energy of 250 MeV/nucleon, employing the cross sections for the radiative capture reaction ^{7}Be(p,γ)^{8}B calculated within the Shell Model Embedded in the Continuum (SMEC) approach. In contrast to the situation at lower beam energies, the Coulomb breakup cross sections are found to be sensitive to the $M1$ transitions. Comparisons of SMEC and single-particle potential model predictions show that the Coulomb breakup cross sections at these high energies are sensitive to the structure model of ^{8}B. Comparison with the preliminary data on the angle integrated spectra reported recently by the GSI group shows that the theory is able to reproduce the absolute magnitude as well as the shape of this data well. The contributions of the $E2$ component strongly depends on the range of the angles of the p − ^{7}Be center of mass with respect to the beam direction, included in the angular integrations of the double differential cross section. If integrations are done over the angular range of 0°-1.87°, the $E2$ multipolarity contributes up to 25 % to the cross sections even for the relative energies of [p − ^{7}Be] below 0.25 MeV. However, these contributions are reduced by an order of magnitude at lower relative energies if the maximum of the angle integration is ∼ 1°.

PACS No. 25.70.De, 25.40.Lw, 96.60.Kx

Typeset using REVTEX

I. INTRODUCTION

The ^{8}B isotope produced in the Sun via the radiative capture reaction ^{7}Be(p,γ)^{8}B is the principal source of the high energy neutrinos detected in the Super-Kamiokande and ^{37}Cl detectors [1]. In fact the calculated rate of events in the former detector (and also in the SNO experiment [2]) is directly proportional to the rate of this reaction measured in the laboratory at low energies ($\sim$ 20 keV) [2]. Unfortunately, the measured cross sections (at relative energies (E_{CM}) of [p − ^{7}Be] > 200 keV) disagree in absolute magnitude and the value extracted by extrapolating the data in the region of 20 keV differ from each other by 30-40 %. This makes the rate of the reaction ^{7}Be(p, γ)^{8}B most poorly known quantity in the entire nucleosynthesis chain leading to the formation of ^{8}B [3].

The Coulomb dissociation (CD) method provides an alternative indirect way to determine the cross sections for the radiative capture reactions at low energies [4–9]. In this method, the radiative capture is reversed by the dissociation of the projectile (the fused system) in the Coulomb field of the target by assuming that the strong interaction between the nuclei is absent and the electromagnetic excitation process is dominated by a single multipolarity (see *e.g.* Refs. [5,8]). However, in the CD of ^{8}B, the contributions of $E2$ and $M1$ multipolarities as well as nuclear breakup can be disproportionately enhanced in certain kinematical regimes [10,11] and a careful investigation [9,12] is necessary to isolate the conditions in which these terms have negligible effect on the calculated breakup cross sections.

For the CD measurements of ^{8}B performed at RIKEN [13–15] at around 50 MeV/nucleon, it was found in a theoretical model [9] that the data are free from nuclear and $E2$ contributions if measurements are limited to $E_{CM} < 0.70$ MeV and to angles of $p-^7$Be c.m. with respect to the beam direction (θ_{CM}) <4°. On the other hand, for measurements at sub-Coulomb energies [16], these contributions turned out to be dominant everywhere [9,17]. Furthermore, the multi-step breakup effects were also found to be quite important at these energies [17,18]

Recently, the Coulomb dissociation of ^{8}B on a ^{208}Pb target has been performed at GSI-Darmstadt at the beam energy of 250 MeV/nucleon [19,20]. The advantages of the CD process at this high energy are: (i) measurements at E_{CM} lower than RIKEN are possible due to certain experimental advantages [19,20]. (ii) the multi-step breakup processes (*e.g.* the Coulomb post-acceleration) are negligible [18,21], and (iii) the nuclear breakup processes are expected to be negligible in comparison to the Coulomb one due to the strong enhancement in the virtual photon spectrum [8,21], an advantage that existed already in the experiments performed at the RIKEN energies in the kinematical regime as mentioned above [9]. At the beam energy of 250 MeV/nucleon, the $E2$ component is expected to be about one third of that found at RIKEN energies although, at the same time, the $E1$ component is also reduced by about one half. But more importantly, the $M1$ component is expected to be enhanced particularly in the first resonance region (0.5 MeV < E_{CM} < 0.65 MeV). This provides an alternative opportunity to test various models of the ^{8}B structure, as they differ in their treatment of the resonance structure of this nucleus [22–25].

The aim of this paper is to perform calculations of the CD of ^{8}B on ^{208}Pb target at the beam energy of 250 MeV/nucleon, using the cross section for the cature reaction ^{7}Be(p,γ)^{8}B calculated within a recently developed realistic shell model which includes coupling between

many particle quasi-bound states and the continuum of one particle scattering states (to be referred as the Shell Model Embedded into the Continuum (SMEC) approach) [26,27]. In order to investigate the sensitivity of the CD process to the structure of ^{8}B, we also perform calculations within a single particle potential model using the parameters ginen by Esbensen and Bertsch (EB) [28]. We compare the results of our calculations with the preminary data on the angle integrated cross sections for this reaction taken recently in an experiment performed at the GSI, Darmstadt [19,20]. We discuss the kinematical regime where the breakup measurements performed at these energies can be reliably used to extract the astrophysical S-factor (S_{17}) for the ^{7}Be(p, γ)^{8}B capture reaction.

The remainder of this paper is organized in the following way. The formalism of the SMEC approach is described in the next section. The formulas used in the calculation of the Coulomb dissociation cross sections are also described here. The results of our numerical calculations and their discussions are presented in Sect. 3, while the summary and conclusions of our work is given in Sect. 4.

II. THE FORMALISM

A. The shell model embedded in the continuum (SMEC)

In the next chapter, we shall study the CD process ^{8}B $\rightarrow$ ^{7}Be $+ p$, using the Shell Model Embedded in the Continuum (SMEC) which has been applied recently to examine structure for mirror nuclei, ^{8}B, ^{8}Li , and capture cross sections for mirror reactions ^{7}Be(p, γ)^{8}B, ^{7}Li(n, γ)^{8}Li [26,27]. The SMEC model, in which realistic Shell Model (SM) solutions for (quasi-)bound states are coupled to the one-particle scattering continuum, is a development of the Continuum Shell Model (CSM) [30–32] for the description of low excitation energy properties of weakly bound nuclei. In the SMEC, the bound (interior) states together with its environment of asymptotic scattering channels form a quantum closed system. Using the projection operator technique, one separates the P subspace of asymptotic channels from the Q subspace of many-body states which are build up by the bound s.p. wave functions and by the s.p. resonance wave functions. P subspace is assumed to contain $(N-1)$ - particle states with nucleons on bound s.p. orbits and one nucleon in the scattering state. Also the s.p. resonance wave functions outside of the cutoff radius R_{cut} are included in the P subspace. The resonance wave functions for $r < R_{cut}$, are included in the Q subspace. The wave functions in Q and P are then properly renormalized in order to ensure the orthogonality of wave functions in both subspaces.

For the (quasi-) bound many-body states in Q subspace one solves the SM problem

$$H_{QQ}\Phi_i = E_i\Phi_i \tag{1}$$

where $H_{QQ} \equiv QHQ$ is the SM effective Hamiltonian. What should be taken for coupling between bound and scattering states is in principle not known and we have decided to use a schematic combination of Wigner and Bartlett forces [27]

$$V_{12} = -V_{12}^{(0)}[\alpha + (1 - \alpha)P_{12}^\sigma]\delta(\mathbf{r}_1 - \mathbf{r}_2) \tag{2}$$

3

where P_{12}^{σ} is the spin exchange term and $(1 - \alpha)$ is the spin exchange parameter. We assume that effects of this coupling on the effective interaction in Q subspace are already contained in H_{QQ}.

The SM wave function has an incorrect asymptotic radial behavior for unbound states. Therefore, to generate both the radial s.p. wave functions in the Q subspace and the scattering wave functions in P subspace we use the average potential of Saxon-Woods (SW) type with the spin-orbit part included

$$U(r) = V_0 f(r) + V_{SO}(4\mathbf{l} \cdot \mathbf{s})\frac{1}{r}\frac{d\rho(r)}{dr} + V_C \tag{3}$$

where $f(r)$ is the spherical symmetric SW form factor

$$\rho(r) = \left[1 + \exp\left(\frac{r - R_0}{a}\right)\right]^{-1} . \tag{4}$$

The Coulomb potential V_C is calculated for the uniformly charged sphere with radius R_0.

For the continuum part, one solves the coupled channel equations

$$(E^{(+)} - H_{PP})\xi_E^{c(+)} \equiv \sum_{c'}(E^{(+)} - H_{cc'})\xi_E^{c'(+)} = 0 \tag{5}$$

where index c denotes different channels and $H_{PP} \equiv PHP$. The superscript $(+)$ means that boundary conditions for outgoing scattering waves are used. The channel states are defined by coupling one nucleon in the scattering continuum to a many-body state of $(N-1)$ - nucleus given by the SM. The channel - channel coupling potential in (5) is

$$H_{cc'} = (T + U)\delta_{cc'} + v_{cc'}^J \tag{6}$$

where T is the kinetic-energy operator and $v_{cc'}^J$ is the channel-channel coupling generated by the residual interaction. U in (6) consists of an 'initial guess' $U(r)$ given by (3) and the diagonal part of the coupling potential v_{cc}^J which depends on both the s.p. orbit $\phi_{l,j}$ and the considered many-body state J^π. Obviously, this correction cannot be neglected when generating s.p. wave function $\phi_{l,j}$ for a given J^π. These s.p. wave functions define Q subspace and thus modify the diagonal part of the residual force. This implies a self-consistent iterative procedure, because the change of s.p. wave function changes the correction coming from the residual force, and so on. This procedure yields the new *self-consistent potential*

$$U^{(sc)}(r) = U(r) + v_{cc}^{J(sc)}(r) \tag{7}$$

and consistent with it the new *renormalized matrix elements* of the coupling force. The parameters of the initial potential $U(r)$ are chosen in such a way that $U^{(sc)}(r)$ reproduces energies of experimental s.p. states, whenever their identification is possible.

The third system of equations in SMEC consists of inhomogeneous coupled channel equations

$$(E^{(+)} - H_{PP})\omega_i^{(+)} = H_{PQ}\Phi_i \equiv w_i \tag{8}$$

with the source term w_i which is primarily given by the structure of N - particle SM wave function Φ_i . The explicit form of this source was given in [27]. These equations define

4

functions $\omega_i^{(+)}$, which describe the decay of quasi-bound state Φ_i in the continuum. The source w_i couples the wave function of N - nucleon localized states with $(N-1)$ - nucleon localized states plus one nucleon in the continuum. Form factor of the source term is given by the self-consistently determined s.p. wave functions.

The full solution is expressed by three functions Φ_i , ξ_E^c and ω_i [27,30]

$$\Psi_E^c = \xi_E^c +$$
$$+ \sum_{i,j}(\Phi_i + \omega_i)\frac{1}{E - H_{QQ}^{eff}} < \Phi_j \mid H_{QP} \mid \xi_E^c > \tag{9}$$

where

$$H_{QQ}^{eff} = H_{QQ} + H_{QP}G_P^{(+)}H_{PQ} \tag{10}$$

is the *effective* SM Hamiltonian which includes the coupling to the continuum, and $G_P^{(+)}$ is the Green function for the motion of s.p. in the P subspace. Matrix H_{QQ}^{eff} is non-Hermitian (the complex, symmetric matrix) for energies above the particle emission threshold and Hermitian (real) for lower energies. The eigenvalues, $\tilde{E}_i - \frac{1}{2}i\tilde{\Gamma}_i$, are complex for decaying states and depend on the energy E of particle in the continuum. The energy and width of resonance states is determined by the condition $\tilde{E}_i(E) = E$ [30]. Inserting them in (9), one obtains

$$\Psi_E^c = \xi_E^c +$$
$$+ \sum_i \tilde{\Omega}_i \frac{1}{E - \tilde{E}_i + (i/2)\tilde{\Gamma}_i} < \tilde{\Phi}_i \mid H \mid \xi_E^c > \tag{11}$$

for the continuum many-body wave function projected on channel c , where

$$\tilde{\Omega}_i = \tilde{\Phi}_i +$$
$$+ \sum_c \int_{\varepsilon_c}^{\infty} dE' \xi_{E'}^c \frac{1}{E^{(+)} - E'} < \xi_{E'}^c \mid H \mid \tilde{\Phi}_i > \tag{12}$$

is the wave function of discrete state modified by the coupling to the continuum states. It should be stressed that the SMEC formalism is *fully symmetric* in treating the continuum and bound state parts of the solution, Ψ_E^c represents the continuum state modified by the discrete states, and $\tilde{\Omega}_i$ represents the discrete state modified by the coupling to the continuum.

B. SMEC wave functions for ^{8}B

The SMEC results depend mainly on (i) the effective nucleon - nucleon interaction in Q subspace, (ii) the residual coupling of Q and P subspaces, (iii) the self-consistent average s.p. potential which generates the radial form factor for s.p. bound wave functions and s.p. resonances. Cohen - Kurath (CK) interaction [33] is used for the SM effective interaction in Q subspace. The freedom of choosing asymptotic conditions in solving eqs. (8) means that the zero on the excitation energy scale can be fixed arbitrarily. We choose the zero

on this scale by requiring that the lowest resonance ($J^{\pi} = 1_1^+$) with respect to the proton emission threshold has its experimental position. An essential element of SMEC approach is the construction of Q - subspace. This is achieved by an iterative procedure which yields the self-consistent s.p. potential depending on the s.p. wave function $\phi_{l,j}$, the total spin J of the N-nucleon system as well as on the one-body matrix elements of $(N-1)$ - nucleon daughter system. The parameters of initial SW potentials for different contributions of spin exchange component in the residual interaction (2) are summarized in Table I.

The unique potential $U(r)$ is used for the calculation of self-consistent potentials for *all many-body states* in ^{8}B, and for both $1p_{3/2}$ and $1p_{1/2}$ proton s.p. states. For neutrons, there is no correction from the residual interaction, and the average s.p. potential is chosen such that it yields $1p_{3/2}$ and $1p_{1/2}$ neutron orbits at -13.02 MeV and -11.16 MeV respectively [27].

The quadrupole moment $< Q >$ of ^{8}B is a useful test of the SMEC wave function. We have calculated $< Q >$ following the approach of Carchidi et al. [34]. For the residual force (2) with $V_{12}^{(0)} = 650$ MeV·fm^3 and for the spin exchange parameter $(1 - \alpha) = 0.05$ one finds [27], $< Q >= 6.99$ e fm^2, in the good agreement with the experimental value [35], $< Q >= 6.83 \pm 0.21$ e fm^2. This theoretical value has been obtained assuming the effective charges, $e_p = 1.35$, $e_n = 0.35$, and the SM spectroscopic factors for the CK interaction.

SMEC results depend sensitively on very small number of parameters. Some of them, like the parameterization of the residual interaction which couples states in Q and P subspaces, has been established previously [26,27]. The others, related to the energy of s.p. states which determine the radial wave function of many-body states, are bound by the SM spectroscopic factors and experimental binding energy in studied nuclei. The spectrum of ^{8}B depends strongly on couplings to the ground state (g.s.) of ^{7}Be but changes very little if also the couplings to the excited state $3/2^-$ of ^{7}Be are taken into account [27]. Width for $J^{\pi} = 1_1^+$ state depends sensitively on the proportion of direct and spin exchange terms (see Table II) in the residual interaction.

Varying the parameter of the spin exchange component for a fixed intensity of the coupling, we came to the conclusion that most satisfactory description of experimental data are achieved for small contribution of the spin exchange part, *i.e.*, approaching the limit of pure Wigner force [36]. This finding is consistent with the results of SM which strongly suggest an approximate validity of $SU(4)$ symmetry in p-shell nuclei [33,37–39].

SM energy of the first $J^{\pi} = 3_1^+$ level is too low as compared to the experimental value (see Table II). The coupling to the continuum cannot correct for this deficiency. The width of 3_1^+ state differs by at least a factor 5 from the experimental data and here, again, the agreement between experiment and calculations improves when $(1 - \alpha) \to 0$. There are several reasons for this discrepancy. Firstly, SM with CK interaction is not well describing energy of this state and, as pointed above, the width of the many-body state depends on its excitation energy with respect to the particle emission threshold (see Table II). Secondly, the wave function of experimental 3_1^+ state is certainly overlapping with the cluster configuration [^{3}He $-$ ^{5}Li], which cannot be adequately described in p-space SM calculations. Experimental 3_1^+ state lies above the threshold for three-particle decay, ^{8}B $\longrightarrow$ [^{3}He $-$ p $-$ ^{4}He]. This decay channel largely contributes to the 3_1^+ width, but cannot be accounted for in the approximation of one-particle scattering continuum. We have to keep in mind these limitations when analyzing the Coulomb dissociation cross-section for ^{8}B .

C. Radiative capture

The calculation of the capture cross-section in the SMEC goes as follows. The initial wave function for $[p \otimes {}^7Be]$ system is

$$\Psi_i(r) = \sum_{l_a j_a} i^{l_a} \frac{\psi_{l_a j_a}^{J_i}(r)}{r} \left[[Y^{l_a} \times \chi^s]^{j_a} \times \chi^{I_t} \right]_{m_i}^{(J_i)} \tag{13}$$

and the final wave function for ${}^8B$ in the g.s. $(J^\pi = 2^+)$ is

$$\Psi_f(r) = \sum_{l_b j_b} A_{l_b s j_b}^{j_b I_b J_f} \frac{u_{l_b j_b}^{J_f}(r)}{r} \left[[Y^{l_b} \times \chi^s]^{j_b} \times \chi^{I_t} \right]_{m_f}^{(J_f)} \tag{14}$$

I_t and s denote the spin of target nucleus and incoming proton, respectively. $A_{l_b s j_b}^{j_b I_b J_f}$ is the coefficient of fractional parentage and $u_{l_b j_b}^{J_f}$ is the s.p. wave in the many-particle state J_f. These SMEC wave functions, $\Psi_i(r)$, $\Psi_f(r)$, are then used to calculate the transition amplitudes $T^{E\mathcal{L}}$ and T^{M1} for $E1$, $E2$ and $M1$ transitions, respectively [26,27]. The radiative capture cross section is

$$\sigma^{E1,M1} = \frac{16\pi}{9} \left(\frac{k_\gamma}{k_p} \right)^3 \left(\frac{\mu}{\hbar c} \right) \left(\frac{e^2}{\hbar c} \right) \frac{1}{2s+1} \frac{1}{2I_t+1} \times$$
$$\times \sum |T^{E1,M1}|^2 \tag{15}$$

$$\sigma^{E2} = \frac{4\pi}{75} \left(\frac{k_\gamma^5}{k_p^3} \right) \left(\frac{\mu}{\hbar c} \right) \left(\frac{e^2}{\hbar c} \right) \frac{1}{2s+1} \frac{1}{2I_t+1} \times$$
$$\times \sum |T^{E2}|^2 \tag{16}$$

where μ stands for the reduced mass of the system.

The astrophysical S-factor (S_{17}) is related to the capture cross section by

$$S_{17}(E_{CM}) = \sigma^{\pi L}(E_{CM}) E_{CM} e^{[2\pi\eta(E_{CM})]}, \tag{17}$$

where $\eta(E_{CM})$ is the Coulomb parameter and πL represents the multipolarity.

1. SMEC results for ${}^7Be(p,\gamma)^8B$

In Fig. 1, we show the astrophysical S-factors (S_{17}) (as defined by Eq. (2.17)) of $E1$ (solid lines), $E2$ (dashed-dotted line) and $M1$ (dashed line) multipolarities as a function of c.m. energy for four versions of SMEC used in the calculations performed in this paper (see also Fig. 7 of Ref. [27]). The parts (a)-(d) show the results obtained with versions I,II,III,IV of the SMEC model respectively. Version I corresponds to the spin exchange parameter $(1-\alpha)$ in the residual coupling (2) equal 0.27. This is the standard value resulting from a fit to the giant dipole resonance in ${}^{16}O$ [30,41]. In version II, $(1-\alpha) = 0.05$, that corresponds to an almost pure Wigner force limit for this coupling. Strength of the

residual interaction in versions I and II of the SMEC model is, $V_{12}^{(0)} = 650$ MeV·fm^3 and the parameters of the initial SW potentials are given in Table I. Versions III and IV are the same as versions I and II respectively except that the resonant $M1$ contribution for the $J^\pi = 3_1^+$ state has been omitted. This resonance has much smaller width than seen in the data due mainly to the missing three-body final state in the continuum, as explained in Sect. II.B. The $M1$ contribution and particularly its resonant part, are strongly dependent on the spin exchange parameter $(1 - \alpha)$ in the residual coupling (2). For $(1 - \alpha) = 0.05$ the resonant part of $M1$ transitions yields $S^{M1} = 20.52$ eV·b at the 1_1^+ resonance energy. This value is proportional to the square of spectroscopic amplitude of p-states, which for the CK interaction is -0.352 and 0.567 for $p_{1/2}$ and $p_{3/2}$ respectively. Ratio of $E2$ and $E1$ contributions at the position of 1_1^+ resonance is $8.15\cdot10^{-4}$ or $7.72\cdot10^{-4}$ depending on whether $(1-\alpha)$ equals 0.27 or 0.05. The experimentally deduced value for this ratio, $6.7^{+2.8}_{-1.9}\cdot10^{-4}$ [40], is consistent with both values of $(1 - \alpha)$. The $E2$ contribution contains both resonant and non-resonant contributions. Their ratio at 1_1^+ resonance is 0.187 (for $(1 - \alpha) = 0.05$), and the contribution from different initial states, $0^+, 1^+, 2^+, 3^+$ and 4^+ is $1.17\cdot10^{-5}$ μb, $7.2\cdot10^{-5}$ μb, $4.64\cdot10^{-5}$ μb, $6.01\cdot10^{-5}$ μb and $5.64\cdot10^{-5}$ μb, respectively. Importance of this quantity has been suggested recently by Barker [42].

$E1$ component provides the main contribution to the total capture cross-section. The low energy behavior of the astrophysical factor $S_{17}(E)$ can be approximated by, $S_{17}(E) = S_{17}(0)\exp(\hat\alpha E + \hat\beta E^2)$. In the range of c.m. energies up to 100 keV, it yields $S_{17}(0) = 19.594$ eV·b, $\hat\alpha = -1.544$ MeV^{-1}, $\hat\beta = 6.468$ MeV^{-2} for $(1 - \alpha) = 0.05$. The above value of $S_{17}(0)$ is close to the values reported by Filippone et al. [43] and Hammache et al. [44]. At the position of 1_1^+ resonance, the calculated S_{17} - factor ($S_{17} = 40.67$ eV·b) is somewhat smaller than that reported by Filippone et al. [43] .

D. Single-particle model for ^{8}B

For a comparison, we shall also study the CD of ^{8}B using a simple s.p. description of loosely bound proton in ^{8}B, using the potential parameters given by Esbensen and Bertsch (EB) [28]. This will be referred to as the EB potential model in the following. The S-factors obtained with this model are shown by lines with solid circles in part (c) of Fig. 1. In this model, both the g.s. 2_1^+ as well as the resonances 1_1^+ and 3_1^+ are assumed to have the structure $[^7\text{Be}(3/2^-)\otimes 1p_{3/2}]$, i.e., the spectroscopic amplitudes for these states are assumed to be equal 1. This assumption is perhaps questionable for the 1_1^+ and 3_1^+ resonances [45] (the experimental spectroscopic factor for 1_1^+ resonance for the mirror state in ^{8}Li is 0.48 [46]). No intrinsic excitations of the ^{7}Be are allowed and the s.p. potential well is adjusted for each state separately to reproduce either the one-proton separation energy (for the g.s. 2_1^+) or the excitation energies (for the 1_1^+ and 3_1^+ resonances). This extreme s.p. description of the ^{8}B yields the width of resonances appreciably bigger than the experimental value, in contrast to the SMEC, which yields too narrow width for those states. For example, the 1_1^+ width in the EB potential model is 70 keV as compared to the measured value 37 ± 5 keV and the 3_1^+ width is 1740 keV instead of 350 ± 40 keV found experimentally [46]. In SMEC widths of 1_1^+ and 3_1^+ states are 26 keV and 35 keV, and 16.5 keV and 13 keV for for $(1-\alpha) = 0.05$ and 0.27 respectively [27].

8

In the EB potential model, the ratio S^{E2}/S^{E1} at the 1^+_1 peak energy equals $9.5 \cdot 10^{-4}$ and situates at the upper most limit of the experimental values deduced by Davids et al. [40]. Ratio of resonant and nonresonant $E2$ contributions at this energy is 0.305. The astrophysical factor $S_{17}(0)$ is $\simeq 18.4$ eV·b and is close to the value in the SMEC approach.

E. Coulomb dissociation cross section

The double differential cross-section for the Coulomb excitation of ^{8}B from its g.s. to the continuum, with a definite multipolarity of order $\pi\lambda$ is given by [4–6]

$$\frac{d^2\sigma}{d\Omega_{8_{B^*}} dE_{CM}} = \sum_{\pi\lambda} \frac{1}{E_{CM}} \frac{dn_{\pi\lambda}}{d\Omega_{8_{B^*}}} \sigma_\gamma^{\pi\lambda}(E_\gamma), \qquad (18)$$

In Eq. (17) $\Omega_{8_{B^*}}$ defines the direction of the c.m. of the $p-^7$Be system (to be referred as ^{8}B*) with respect to the beam direction. $\sigma_\gamma^{\pi\lambda}(E_\gamma)$ is the cross-section for the photo-disintegration process $\gamma + ^8$B $\rightarrow ^7$Be $+ p$, with photon energy E_γ, and multipolarity $\pi = $ E (electric) or M (magnetic), and $\lambda = 1, 2...$ (order), which is related to that of the radiative capture process ^{7}Be $+ p \rightarrow ^8$B $+ \gamma$ through the theorem of detailed balance. E_γ is given by $E_{CM} = E_\gamma + Q$, with $Q = 0.137$. In most cases, only one or two multipolarities dominate the radiative capture as well as the Coulomb dissociation cross sections. $n_{\pi\lambda}(E_\gamma)$ in Eq. (18) represents the number of equivalent (virtual) photons provided by the Coulomb field of the target to the projectile, which is calculated by the methods discussed in Ref. [6,29].

III. RESULTS AND DISCUSSION

In Fig. 2, we show the results of the calculations for the energy differential cross sections for the reaction ^{8}B $+ ^{208}$Pb $\rightarrow ^8$B$^* + ^{208}$Pb at the beam energy of 250 MeV/nucleon, using the capture cross sections obtained with versions I, II, III, IV of SMEC.

Results shown in Fig. 2 have been obtained by integrating Eq. (18)) for $\theta_{8_{B^*}}$ angles from 0.01° - 1.87°, which is the range of the angle integration in the preliminary GSI data as reported in [19,20]. The cross sections for $E1$, $E2$ and $M1$ multipolarities are shown by dashed, dotted and dashed-dotted lines respectively, while the solid line shows their sum. We note that all the four models reproduce the preliminary GSI data (which has been taken from the thesis of Federick Boue [19]) well. However, in models I and II, a peak appears at $E_{CM} \sim 1.2$ MeV. This is because these models include also the contributions from the 3^+ state in the ^{8}B continuum which in SMEC occurs at about 1.2 MeV excitation energy. This gives rise to a strong resonance in the $M1$ capture cross sections which is reflected in the corresponding Coulomb dissociation results. In models III and IV, contributions from this state is not included. In each case, the $E2$ multipolarity contributes to the extent of about 25%. The maximum in the experimental cross sections is around $E_{CM} = 0.5$ MeV. The calculations cannot reproduce this without strong contributions from the $M1$ multipolarity, as will be shown later on.

In Fig. 3, we present the comparison of the Coulomb dissociation cross sections (for the same reaction as in Fig. 2), obtained with capture cross sections of versions III (a) and IV (b) of the SMEC model and the EB potential model. The results for $E1$, $E2$ and $M1$

multipolarities for SMEC models and the EB potential model are shown by dashed-dotted and dotted lines respectively. Their sum is shown by the solid and dashed lines in the two cases. We note that the SMEC cross sections are in somewhat better agreement with the preliminary GSI data. As compared to SMEC, the EB calculations under-predict the experimental data for E_{CM} larger than about 0.8 MeV, while they over-predict it around the 1^+ resonance region. This can be traced back to the differences in predictions of the two models for the direct capture cross sections of various multipolarities (see Fig. 1). We note that while the $E1$ cross sections obtained with SMEC (version III) and EB model are similar, the two differ in case of SMEC version IV. On the other hand, SMEC E2 cross sections are always larger than that of the EB potential model. At the same time, the $M1$ cross section of the latter are much larger and wider in width as compared to that of former.

Therefore, the Coulomb dissociation data at these high energies seem to show sensitivity to the capture cross sections calculated within different models of ^{8}B structure. Although these are only preliminary data, yet SMEC models appear to be in a somewhat better agreement with it. Unfortunately, it is difficult to commment on the the difference seen in the widths of the $M1$ resonance in the two models. This is because the experiments have a finite resolution ($\sim$ 110 keV at $E_{CM} = 0.63$ MeV [20]) that may give a large aparent width to the cross sections near the resonance region. Furthermore, the data are presented in the larger energy bins. It would, be worthwhile to improve upon both these aspects in the future studies. However, it must be added here that the width of this resonance is tested basically with the direct radiative capture (p, γ)data.

We next investigate the role of the $M1$ multipolarity in the high energy data of GSI. We would like to recall that at lower beam energies (e.g., the RIKEN experiments [13,14]), the contribution of this multipolarity was almost negligible. In Fig. 4, we show the CD predictions (obtained with SMEC, version III) for $E1$, $E2$ and $M1$ components of the angular distributions for the ^{8}B + ^{208}Pb $\rightarrow$ ^{8}B* + ^{208}Pb reaction at the beam energies of 51.9 MeV/nucleon. For completeness sake we also show the experimental data of Kikuchi et al. [14]. Note that since these CD calculations have been done within a pure semi-classical theory [47], the agreement with the data, beyond 4° is not good as compared to that seen in Ref. [9]. As has been discussed in Ref. [9], the point like projectile approximation of the semi-classical theory breaks down at angles beyond this. Inclusion of finite-size effects of the projectile reduces the cross sections at larger angles which leads to a better agreement with the experimental data [9]. It may remarked here that although, the calculations reported in Ref. [14] are done within a quantum mechanical theory, the point like projectile approximation is still made there. Any how, the purpose of this figure is more to show the contribution of the $M1$ multipolarity to the CD cross sections. As can be seen, the contribution of this multipolarity is negligible even in the energy bin 500-750 keV.

On the other hand, one can see from Fig. 5, where we show the CD calculations for only $E1$ (dashed lines) and $E2$ (dotted lines) multipolarities and their sum (solid line) for the same reaction as in Fig. 2, that at 250 MeV/nucleon, it is not possible to explain the data in the region of E_{CM} between 500-750 keV without the contribution of the $M1$ multipolarity. In this figure the results obtained with versions III (a) and IV (b) of SMEC are shown. The $E1 + E2$ cross sections in version IV are somewhat larger as the $E1$ component in this case is bigger. This sensitivity of the higher energy breakup data to the $M1$ multipolarity makes it possible to use this to supplement the information on the continuum structure of ^{8}B which

was not feasible by similar studies at lower beam energies.

In Fig. 6, we show the CD angular distributions (θ in this figure corresponds to $\theta_{8_{B^*}}$) calculated with capture cross sections of SMEC versions III and IV for the same reaction as in Fig. 2. These results have been obtained by integrating Eq. (18) over E_{CM} between 0.1 MeV to 3.0 MeV. The contributions of $E1$, $E2$ and $M1$ multipolarities are shown by by dashed, dotted and dashed-dotted curves respectively. Their sum is shown by the solid lines. We can see that $E2$ and $M1$ contributions start becoming important already from $1°$. Therefore, the requirement of the CD method that for a reliable extraction of the astrophysical S-factor the data should be dominated by the excitation of a single multipolarity ($E1$ in present case), is more likely to be fulfilled in the measurements at GSI energies if the angle $\theta_{8_{B^*}}$ is kept below $1°$.

This point is further emphasized in Fig. 7, where we show the energy distributions of the CD cross sections obtained by integrating Eq. (17) for $\theta_{8_{B^*}}$ up to $1.87°$ (angular range of the data used in this paper) (part (a)), and that obtained by performing the integration up to $1°$ only (part (b)).

The $E1$, $E2$ and $M1$ components are shown by dashed, dotted and dashed-dotted curves respectively, while their sum is shown by the solid curves. The cross sections are shown only up to E_{CM} of 0.5 MeV, which is the region of interest for the determination of the S-factor. It can be seen from part (a) that if $\theta_{8_{B^*}}$ goes up to $1.87°$, the $E2$ components are substantial (up to about 25%) even at E_{CM} below 0.25 MeV. However, if $\theta_{8_{B^*}}$ is confined to angles below $1°$, the contributions of the $E2$ component are almost an order of magnitude down in comparison to those of $E1$ for E_{CM} below 0.30 MeV. Therefore, this provides a better possibility of a reliable extraction of S_{17}.

IV. SUMMARY AND OUTLOOK

In this paper, we used the cross sections for the radiative capture reaction $^7\text{Be}(p,\gamma)^8\text{B}$, calculated within the shell model embedded into the continuum approach for the structure of ^8B, to study the Coulomb dissociation of ^8B on a ^{208}Pb target at the beam energy of 250 MeV/nucleon. Cross sections obtained with four versions of SMEC were used. Calculations were also performed with the capture cross sections obtained in a single particle model using the potential parameters given by Esbensen and Bertsch [28]. Comparison of the calculations were made with the preliminary data for this reaction taken at GSI, Darmstadt recently.

The CD cross sections at these high energy were found to be sensitive to the nuclear structure model of ^8B. In contrast to the CD data taken at lower beam energies, the $M1$ multipolarity is quite important at higher beam energies. It may therefore, be possible to supplement the information on the continuum structure of ^8B from the CD studies at higher energies. As far as the preliminary data are concerned, the fits obtained with SMEC approach are somewhat better than those with the EB potential model. We noted that if the angles of the center-of-mass of the outgoing $[\text{p}-^7\text{Be}]$ pair with respect to the beam direction were taken up to $1.87°$, the $E2$ component is quite large even at $[\text{p}-^7\text{Be}]$ CM energies below 0.25 MeV. To minimize the contribution of the $E2$ multipolarity, this angle should be confined to values below $1°$. This conclusion appears to be by and large independent of the nuclear structure model of ^8B.

ACKNOWLEDGMENTS

REFERENCES

[1] J.N. Bahcall, Neutrino Astrophysics, Cambridge University Press, New York (1989); J.N. Bahcall, M.H. Pinsonneault, Rev. Mod. Phys. **69** (1995) 781.

[2] J.N. Bahcall, Nucl. Phys. **A 631** (1998) 29.

[3] E.G. Adelberger et al., Rev. Mod. Phys. **70** (1998) 1265.

[4] G. Baur, C.A. Bertulani and H. Rebel, Nucl. Phys. **A 458** (1986) 188.

[5] G. Baur and H. Rebel, J. Phys.G : Nucl. and Part. Phys. **20** (1994) 1.

[6] R. Shyam, I.J. Thompson and A.K. Dutt-Majumder, Phys. Lett. **B 371** (1996) 1.

[7] R. Shyam and I.J. Thompson, Phys. Lett. **B 415** (1997) 315.

[8] G. Baur and H. Rebel, Ann. Rev. Nuc. Part. Sc. **46** (1997) 321.

[9] R. Shyam and I.J. Thompson, Phys. Rev. **C 59** (1999) 2465.

[10] K. Langanke and T.D. Shoppa, Phys. Rev. **C 49** (1994) R1771; **C 51** (1995) 2844(E); **C 52** (1995) 1709.

[11] M. Gai and C.A. Bertulani, Phys. Rev. **C 52** (1995) 1706.

[12] C.A. Bertulani and M. Gai, Nucl. Phys. **A 636** (1998) 227.

[13] T. Motobayashi et al., Phys. Rev. Lett. **73** (1994) 2680.

[14] T. Kikuchi et al., Phys. Lett. **B 391** (1997) 261.

[15] T.Kikuchi et al., Eur. Phys. J. A **3** (1998) 213.

[16] Johanes von Schwarzenberg *et al.*, Phys. Rev. **C 53** (1996) R2598.

[17] F.M. Nunes and I.J. Thompson, Phys. Rev. **C 57** (1998) R2818; Phys. Rev. **C 59** (1999) 2652.

[18] S. Typel, H.H. Wolter and G. Baur, Nucl. Phys. **A 613** (1997) 147.

[19] F. Boué, Ph.D. Thesis, University of Bordeaux 1, Centre d'Etudes Nucléaires de Bordeaux - Gradignan, Report C.E.N.B.G. 99-03.

[20] N. Iwasa et al., Phys. Rev. Lett. **83** (1999) 2910.

[21] C. Bertulani, Nucl. Phys. **A 587** (1995) 318.

[22] A. Csótó, LANL preprint nucl-th/9908081; A. Csótó and K. Langanke, Nucl. Phys.A **636** (1998) 240.

[23] F.M. Nunes, R. Crespo and I.J. Thompson, Nucl. Phys.A **615** (1997) 69.

[24] D.V. Fedorov, E. Garrido, and A.S. Jensen, Phys. Rev.C **51** (1995) 3052.

[25] P. Descouvemont and D. Baye, Nucl. Phys.A **567** (1994) 341.

[26] K. Bennaceur, F. Nowacki, J. Okołowicz, and M. Płoszajczak, J. Phys. **G 24** (1998) 1631.

[27] K. Bennaceur, F. Nowacki, J. Okołowicz, and M. Płoszajczak, Nucl. Phys. **A 651** (1999) 289.

[28] H. Esbensen and G.F. Bertsch, Nucl. Phys. **A 600** (1996) 37.

[29] A.N.F. Alexio and C.A. Bertulani, Nucl. Phys. **A 505** (1989) 448.

[30] H.W. Bartz, I. Rotter, and J. Höhn, Nucl. Phys. **A 275** (1977) 111.

[31] H.W. Bartz, I. Rotter, and J. Höhn, Nucl. Phys. **A 307** (1977) 285.

[32] H.R. Kissener, I. Rotter, and N.G. Goncharova, Fortschr. Phys. **35** (1987) 277; I. Rotter, Rep. Prog. Phys. **54** (1991) 635.

[33] S. Cohen and D. Kurath, Nucl. Phys. **A 73** (1965) 1.

[34] M. Carchidi, B.H. Wildenthal and B.A. Brown, Phys. Rev. **C 34** (1986) 2280.

[35] T. Minamisono et al., Phys. Rev. Lett. **69** (1992) 2058.

[36] E. Wigner, Phys. Rev. **51** (1937) 106.

[37] P.T. Nang, Nucl. Phys. **A 185** (1972) 413.

[38] N.C. Mukhopadhyay and F. Cannata, Phys. Lett. **B 51** (1974) 225.

[39] G. John and P. Kramer, Nucl. Phys. **A 204** (1973) 203.

[40] B. Davids et al., Phys. Rev. Lett. **81** (1998) 2209.

[41] B. Buck and A.D. Hill, Nucl. Phys. **A 95** (1967) 271;
I. Rotter, private communication.

[42] F.C. Barker, private communication.

[43] B.W. Filippone et al., Phys. Rev. Lett. **50** (1983) 452.

[44] F. Hammache et al., Phys. Rev. Lett. **80** (1998) 928.

[45] F.C. Barker, Phys. Rev. **C 37** (1988) 2920.

[46] F. Ajzenberg-Selove, Nucl. Phys. **A 490** (1988) 1.

[47] K. Alder and A. Winther, *Electromagnetic Excitation* (North-Holland, Amsterdam, 1975).

TABLE I. Parameters of the initial potentials $U(r)$ (3) used in the calculations of self-consistent potentials $U^{(sc)}(r)$ for two parameters $(1-\alpha)$ of the spin exchange term in the residual interaction (2). All these potentials have the same parameters of radius $R_0 = 2.4$ fm, surface diffuseness $a = 0.52$ fm, and spin-orbit coupling $V_{SO} = -4$ MeV. In all cases, the strength of the residual interaction (2) is $V_{12}^{(0)} = 650$ MeV·fm^3 [2].

System	$\varepsilon_{p_{3/2}}$ [MeV]	$1-\alpha$	V_0 [MeV]
[p $\otimes$ ^{7}Be]	-0.137	0.27	-40.045
		0.05	-37.660

TABLE II. The dependence of ^{8}B spectra on the relative strengths of direct and spin exchange parts of the residual interaction (2). Only ground state of ^{7}Be was taken into account in all couplings. The proton separation energy is adjusted in order to reproduce the energy of the lowest resonance state 1_1^+. The entries in this table are labelled by the value of the spin exchange parameter $(1-\alpha)$ of the residual force. Strength of the residual interaction (2) is, $V_{12}^{(0)} = 650$ MeV·fm^3. The cut-off radius is $R_{cut} = 5$ fm except for the $p_{1/2}$ s.p. wave function in 1_1^+ many body states, which is in the continuum at about 300 keV above the threshold and for which larger cut-off was used $R_{cut} = 10$ fm. The numbers in parentheses are the widths of 3_1^+ state if this state would be placed at the experimental energy. All units are in keV.

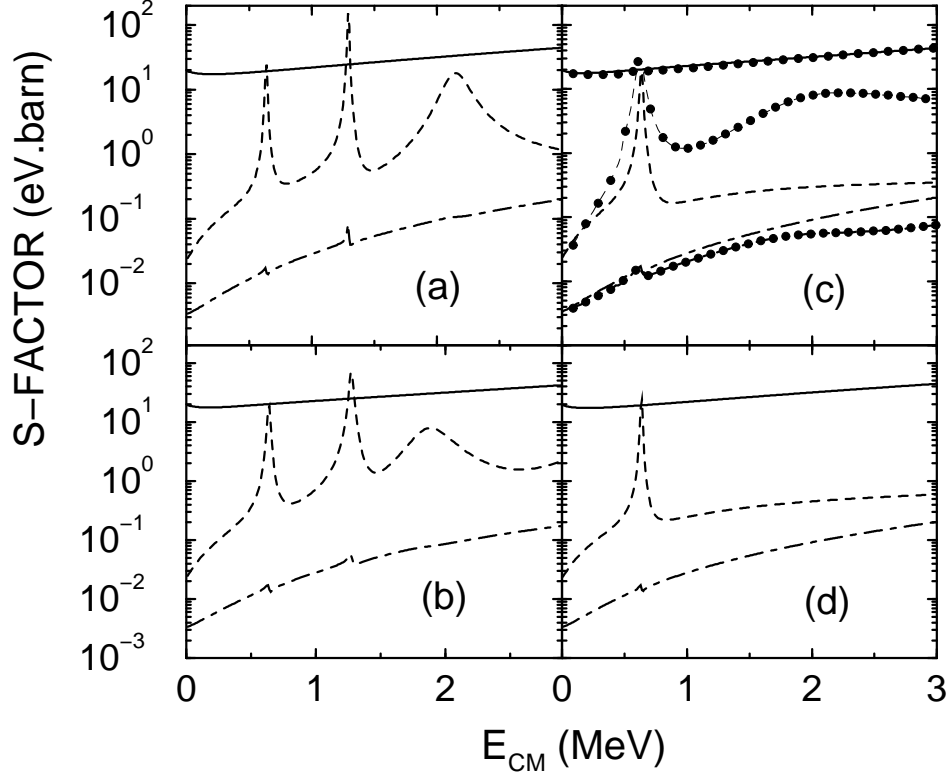| State	SM	$(1-\alpha) = 0.73$		$(1-\alpha) = 0.95$		experiment	
J^π	energy	energy	width	energy	width	energy	width
2^+	-446	-356	—	-320	—	-137.5 ± 1.0	—
1^+	637	637	16.5	637	25.9	637 ± 6	37 ± 5
3^+	1246	1294	13.1	1275	34.9	2183 ± 30	350 ± 40
			(25.2)		(67.4)		

FIG. 1. The astrophysical S-factors for the radiative capture reaction ^{7}Be(p,γ)^{8}B calculated with versions I, II, III and IV of the SMEC (shown in parts (a), (b), (c) and (d) respectively). Solid, dashed-dotted, and dashed curves represent the contributions of $E1$, $E2$ and $M1$ multipolarities respectively. The results obtained with a single particle model with potential parameters taken from [28] are also shown together with model III. The $E1$, $E2$ and $M1$ cross sections in this case are shown by the solid, dashed and dotted lines with solid circles.

^{8}B + ^{208}Pb 250 MeV/nucleon
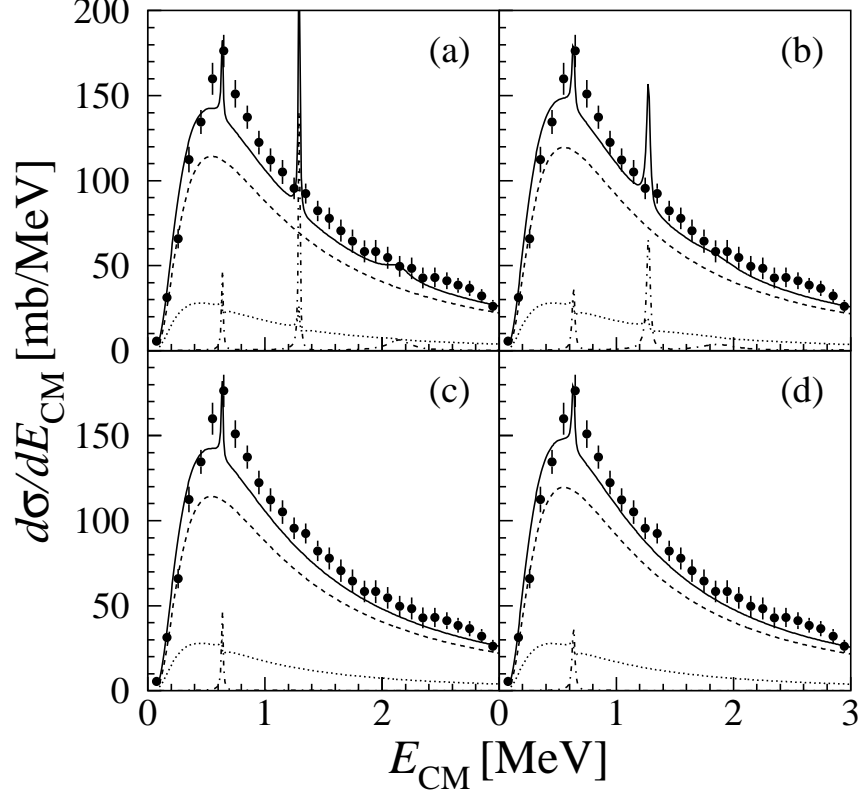
FIG. 2. Comparison of the calculated Coulomb dissociation cross sections ($d\sigma/dE_{CM}$) with the experimental data for the breakup of ^{8}B on ^{208}Pb target at 250 MeV/nucleon, as a function of the $p -^7 Be$ CM energy. The results calculated with four versions of the SMEC are shown (models I, II, III and IV in parts **(a)**, **(b)**, **(c)** and **(d)** respectively). Dashed, dotted and dashed-dotted curves represent the contributions of $E1$, $E2$ and $M1$ multipolarities respectively, while their sum is shown by the solid line. The experimental data are taken from the Ref. [19]. These results have been obtained by integrating the double differential cross sections for angles in the range of $0.0°$-$1.87°$.

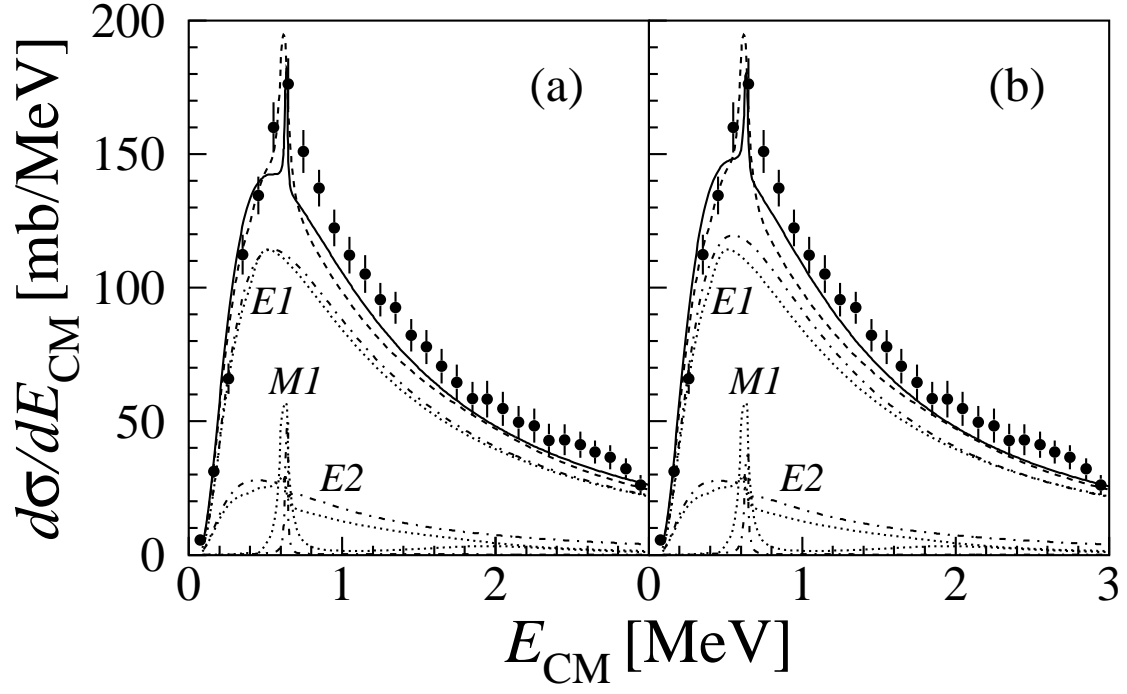^{8}B + ^{208}Pb 250 MeV/nucleon

FIG. 3.   Comparison of the CD calculations (for the same reaction and procedure as in Fig. 1) performed with the capture cross sections obtained with versions III (part **(a)**) and IV (part **(b)**) of the SMEC with those given by the EB single particle model [28]. The $E1$, $E2$ and $M1$ components of the SMEC and EB models are shown by dotted and dashed-dotted lines respectively, while the sum of these components are shown by solid (SMEC) and dashed (EB) lines.
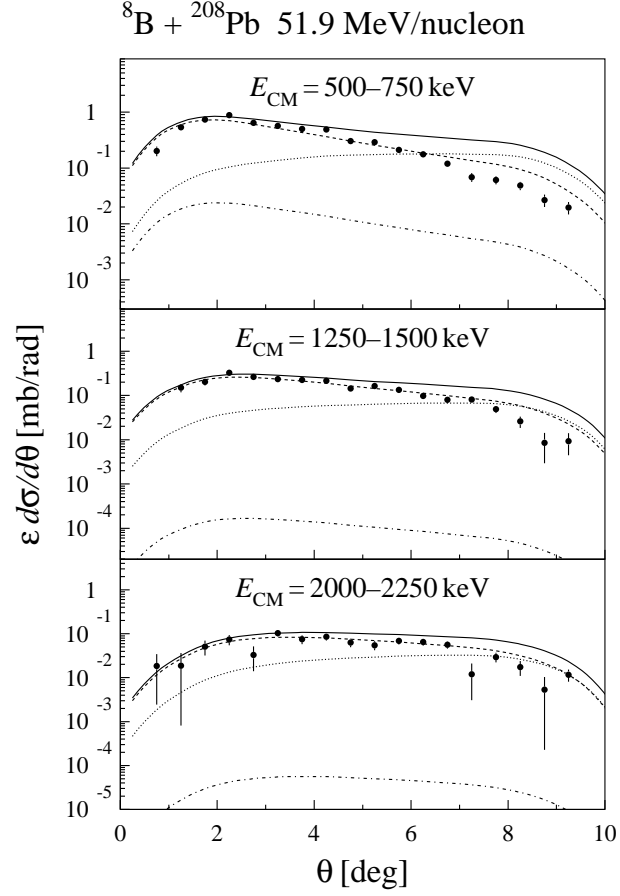
FIG. 4. $E1$ (dashed line), $E2$ (dotted line) and $M1$ (dashed dotted line) components of the Coulomb dissociation cross section $\varepsilon d\sigma/d\theta$ (calculated with version III of SMEC) as a function of the scattering angle θ of $^{8}B^{*}$ for the dissociation of ^{8}B on ^{208}Pb target at the beam energy of 51.9 MeV/nucleon. The solid line shows their sum. Results for the relative energy bins of (a) 500-750 keV, (b) 1250-1500 keV, (c) 2000-2250 keV are shown. ε is the detector efficiency. The experimental data and the detector efficiencies are taken from [14].

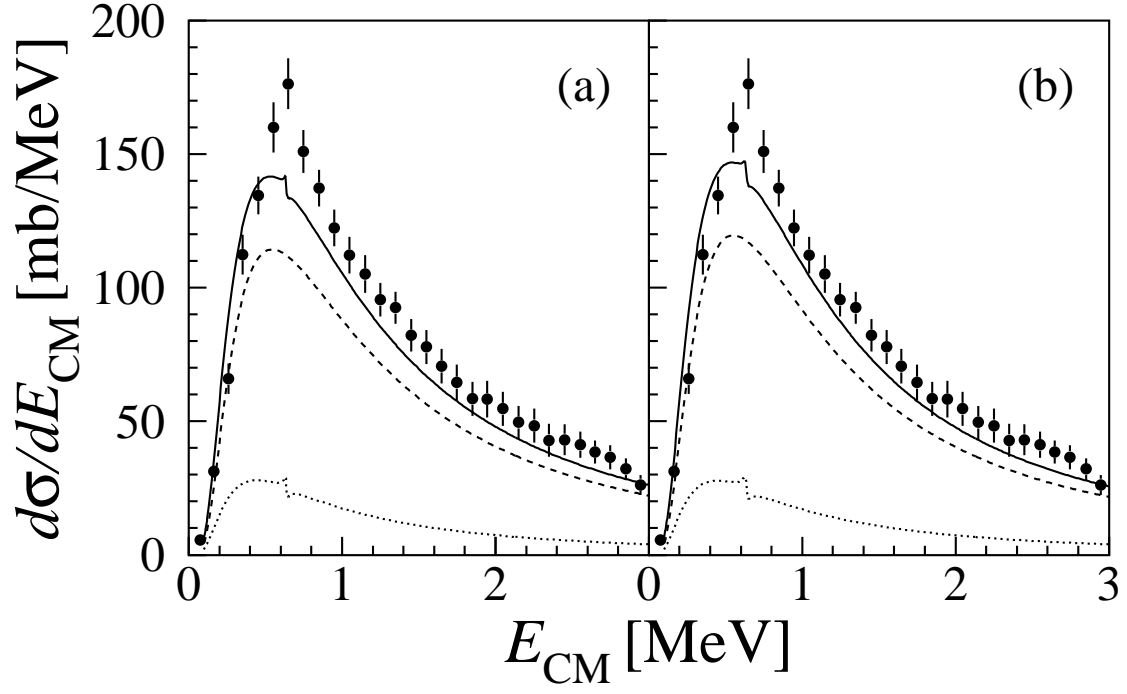$^8\text{B} + \,^{208}\text{Pb}$ 250 MeV/nucleon

FIG. 5. Comparison of the $E1 + E2$ (solid lines) CD cross sections calculated with the capture cross sections of versions III (part **(a)**) and IV (part **(b)**) of SMEC with the experimental data for the same reaction as in Fig. 1. The individual $E1$ and $E2$ components are shown by dashed and dotted lines respectively.
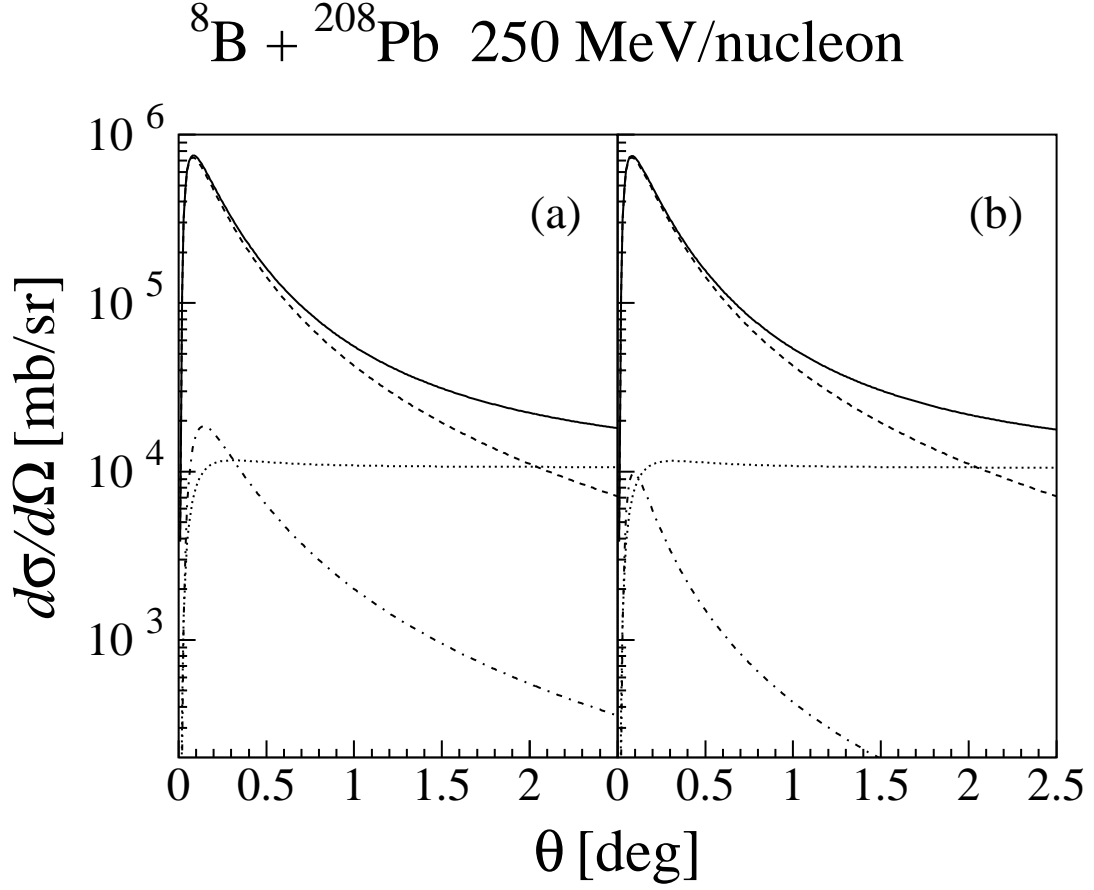
FIG. 6. Angular distributions for the CD of ^{8}B on ^{208}Pb at 250 MeV/nucleon calculated with versions III (part **(a)**) and IV (part **(b)**) of SMEC. These results have been obtained by integrating the double differential cross sections over the CM energies E_{CM} between 100 keV - 3.0 MeV.

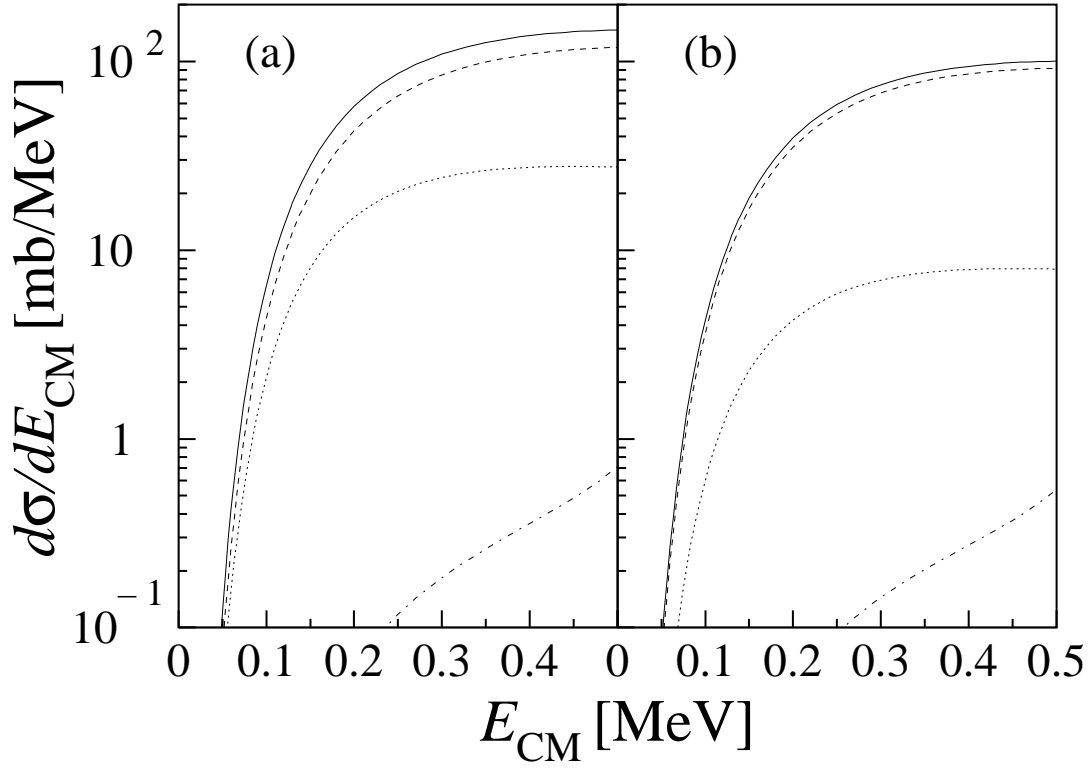$^{8}\text{B} + {}^{208}\text{Pb}$ 250 MeV/nucleon

FIG. 7. The Coulomb dissociation cross sections, $d\sigma/dE_{CM}$, obtianed by integrating the double differential cross sections in the range of 0.01°-1.87° (part (a)) and 0.01°-1.0° (part (b)). The $E1$, $E2$ and $M1$ components are shown by dashed, dotted and dashed-dotted lines respectively while their sum is depicted by the solid lines.